Parallel multi-time point cell stimulation and lysis on-chip for studying early signaling events in T cell activation

Alison M. Hirsch,[a] Catherine A. Rivet,[b] Boyang Zhang,[a] Melissa L. Kemp[bcd] and Hang Lu*[abc]

Received 27th June 2008, Accepted 14th October 2008
First published as an Advance Article on the web 20th November 2008
DOI: 10.1039/b810896j

Dynamics of complex signaling networks are important to many biological problems. Quantitative data at early time points after cellular stimulation are necessary for accurate model generation. However, the large amount of data needed is often extremely time-consuming and expensive to acquire with conventional methods. We present a two-module microfluidic platform for simultaneous multi-time point stimulation and lysis of T cells for early time point signaling activation with a resolution down to 20 s using only small amounts of cells and reagents. The key design features are rapid mixing of reagents and uniform splitting into eight channels for simultaneous collection of multi-time point data. Chaotic mixing was investigated *via* computational fluid dynamic modeling, and was used to achieve rapid and complete mixing. This modular device is flexible—with easy adjustment of the setup, a wide range of time points can be achieved. We show that treatment in the device does not elicit adverse cellular stress in Jurkat cells. The activation of six important proteins in the signaling cascade was quantified upon stimulation with a soluble form of α-CD3. The dynamics from device and conventional methods are similar, but the microdevice exhibits significantly less error between experiments. We envision this high-throughput format to enable simple and fast generation of large sets of quantitative data, with consistent sample handling, for many complex biological systems.

Introduction

Understanding the dynamics of cell signaling networks is important to many biological applications, especially in complex disease phenotypes related to cancer, immune responses, development, and potential pharmacological interferences. Pathways involved in cell maintenance and apoptosis are studied extensively to understand cancer development.[1,2] Focus on particular signal-transduction cascades and molecules has provided system-level insights into mechanism-based drug discovery.[3,4] Building a system-level computational model and gaining insights into the complex signaling networks require large data sets, presently a bottleneck in the process. For example, gene expression patterns or protein activity at various time points during stimulation with an external signal must be known; it usually takes many labs years to accumulate a large body of this type of data.[5–7] Another challenge in signaling research is that many of these important protein activation events, such as phosphorylation, occur within minutes after stimulation.[8–10] Quantitative data not only at precise time points but early in the cells' response are necessary for accurate model generation.

Intracellular immunostaining techniques *via* flow cytometry have proven useful for studying signaling pathways;[11] however, the multi-laser cytometers are constrained for the number of proteins monitored. Cell lysis and biochemical detection of population averages remain the most widespread method of capturing intracellular signaling dynamics of protein pathways. To extract the necessary protein information the cell must be stimulated for a precise period of time and immediately lysed to extract intracellular proteins for downstream analysis. With conventional, multi-well plate assays it is difficult to achieve adequate resolution at sub-minute timescales. Microfluidics is a capable alternative, providing uniformity in sample handling to reduce error between experiments. Moreover, microfluidic systems require relatively small sample volumes for experiments, conserving valuable cells and reagents.[12] Many microdevices have been reported for culturing cells, stimulating with soluble factors, assaying gene expression and performing lysis.[13–22]

The challenges of any on-chip assays are that the devices should minimize stress on the cells, should provide reproducible results from experiment to experiment, should produce quantitative results comparable to or better than bench-top schemes, should be scalable to high-throughput format, should minimize consumption of cells and reagents, and ideally provide the temporal resolution that the bench-top counterparts cannot achieve. So far no chip-based designs have achieved all these criteria simultaneously. Here we present a lab-on-a-chip platform for multiple time point lymphocyte stimulation and lysis for downstream analysis of protein activation. Mixing and even splitting of reagents into each time point channel are key features of the design.

Previously El-Ali *et al.* developed a device achieving cell stimulus and lysis on a microfluidic chip using segmented

[a]*School of Chemical and Biomolecular Engineering, Georgia Institute of Technology, 311 Ferst Drive, N.W., Atlanta, GA, 30332-0100, USA. E-mail: hang.lu@chbe.gatech.edu; Fax: +1 404 894 4200; Tel: +1 404 894 8473*
[b]*Interdisciplinary Program in Bioengineering, Georgia Institute of Technology, USA*
[c]*The Petit Institute for Bioengineering and Biosciences, Georgia Institute of Technology, USA*
[d]*The Wallace H. Coulter Department of Biomedical Engineering, Georgia Institute of Technology and Emory University, USA*

gas–liquid flow for rapid mixing.[16] This device was the first to demonstrate on-chip multiple step manipulation of cells with fast mixing, thereby allowing access to the early time point detection of protein states. For our application, however, to understand over time how multiple proteins in the signaling network behave upon stimulation, vastly different incubation periods are required. Therefore, we have designed our device for eight time points in parallel with controlled rapid mixing, precisely timed stimulation, and rapid lysis. In addition, in this work we also circumvent the large shear at the gas–liquid interface in the earlier work. We show that our assay platform does not induce stress responses to the cells and yields reproducible and quantitative protein activity information with small numbers of cells.

Experimental design

In order to achieve precise incubation control on multiple timescales, we took a two-module approach for increased system flexibility (Fig. 1). In our design, pressure-driven flow (by syringe pumps) entered at only three inlets—cells, stimulus and lysis buffer—which made handling multiple samples and parallel experiments simple. Cells and stimulus were mixed and split into eight equal streams in less than 0.25 s on Module 1. The majority of the incubation time (~20 s to 5 min in our experiments) occurred in the tubing leading to Module 2. On Module 2 the reaction was quenched and cells were lysed by mixing with cold lysis buffer, in less then 1 s, to extract intracellular components. Mixing and balancing flow rates were important to the design, which we describe below.

Rapid mixing to ensure precise stimulation times

For precise definition of stimulation time, especially for the very early time points (*e.g.* 20 s), rapid mixing of cells with reagents was essential to our design. Mixing is necessary in multiple steps of the assay: the cells first have to be mixed with the stimulant, and then once incubated for the desired duration they have to be mixed again with lysis buffer to yield lysate for downstream biochemical assays. If mixing takes a significant portion of the time compared to stimulation and lysis incubation, cells suspended in the initial medium will be introduced to the stimulant at different times, and the contact time cannot be precisely controlled. This non-uniformity of contact time would make it difficult to define and repeat the "stimulation time".

We considered a few existing designs of microfluidic mixers. El-Ali *et al.* have shown a gas–liquid segmented flow scheme to enhance mixing.[16] The advantage of this mixing scheme is that it is very fast and the throughput is high; however, because the mixing scheme relies on the circulation of the liquid behind gas bubbles, the shear is large at the multiphase interface and can introduce undesired lysis and/or mechanotransduction in cells. Ugaz and co-workers[23] demonstrated Dean flow mixing, which is simple and could be suitable for many biological experiments since it is gentle. However, for Dean flow mixers, better mixing correlates to higher Reynolds numbers ($Re = \rho v L/\mu$ where ρ is the density of the fluid, μ the viscosity, v the linear velocity, and L the channel's limiting dimension, is a measure of the inertial effect over viscous effect of fluid flow). To implement this mixing scheme for our application would require large flow rates that render the subsequent incubation step impractical.

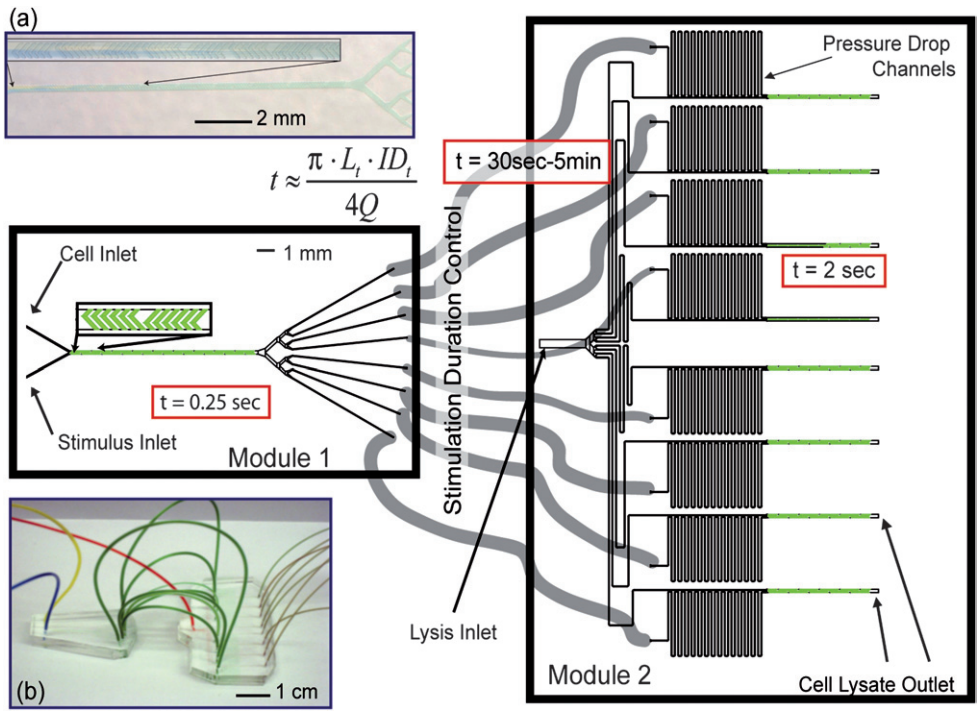

Fig. 1 A schematic of the devices showing inlets, tubing, pressure drop channels and cell lysate outlets for sample collection. The respective residence times (t) in each unit are noted in red boxes on the figure, where the total time is essentially the time in the tubings, varying with length (L), inner diameter (ID) and volumetric flow rate (Q). Insets (a) shows a close-up of Module 1 and (b) the whole device setup.

We chose the asymmetric herringbone mixer (HBM).[24] The mixing time in these devices are sufficiently short for our application and the shear is minimal. There is no analytical solution to the mixing scheme, and a limited number of experiments have been performed on such mixer designs.[25–27] Optimized parameters, asymmetry of the herringbones (2/3 of the way across the channel) and angle with respect to *y*-axis (45°), from Stroock *et al.* were used as a starting point in this design.[24]

In order to design proper mixers for our application and determine an accurate starting time of incubation, we developed computational fluid dynamics (CFD) models for different geometries and experimental flow conditions using COMSOL (Stockholm, Sweden), a finite element solver for non-linear partial differential equations. Because our buffers, cell solutions, and stimulation solutions can have different fluidic properties, the model was also used to probe the mixing effects of viscosity and density. Further confocal microscopy experiments were used to visualize the mixing of solutions with mismatched viscosity.

Flow splitting and precisely-controlled stimulation

After mixing, the fluid was split into eight streams on Module 1. Each stream accomplished a different time point in the tubing leading to Module 2. For efficient device operation, it was necessary for equal volumes of sample to be collected for each time point. Equal flow rates in each stream were achieved by balancing the channel resistance. The resistance, proportional to fluidic pressure drop and a function of channel dimensions, increases with increasing length and decreasing cross-sectional area. From the Hagen–Poiseuille equation,

$$\Delta P = \frac{128\mu QL}{\pi d^4} \quad (1)$$

where ΔP is pressure drop, μ is viscosity, Q is volumetric flow rate, L is path length, and d is the diameter, we calculated a relationship for resistance (R) based on channel dimensions.

$$R \propto \frac{L}{d^4} \quad (2)$$

Since the microfluidic channels are square, when implementing these equations a hydrodynamic diameter was used,

$$d = \frac{2hw}{h+w} \quad (3)$$

where h is the channel height and w is the channel width. This hydrodynamic diameter definition neglects the effect of channel shape,[28] but suits our application in determining the order of magnitude resistance differences between tubing and channels. All the lengths and widths are the same in each time point channel to achieve equal resistance.

The stimulation time is defined by residence time in the device. This time is the sum of the residence time in the channels and the residence time in the tubing leading to the lysis module (Module 2).

$$t = \frac{L_c h_c w_c}{Q} + \frac{L_t \pi \mathrm{ID}_t^2}{4Q} \quad (4)$$

The subscripts c and t denote channels and tubing, respectively, and ID is the inner diameter.

This modular design, as shown in Fig. 1, created a more flexible system by using interchangeable tubing of different lengths and diameters for multiple time point options. The majority of the incubation time occurred in the interchangeable tubing. However, the flow rates must not be influenced when changing lengths or diameters of tubing. This is inherent in our system design because of the small dimensions of the microfluidic channels and the d^4 dependence in the denominator in Eqn (1) and (2). In the worst case scenario with dimensions used in our experimental setup, the channel resistance was still four orders of magnitude greater than that of the tubing. Furthermore, additional long pressure drop channels were added to increase this effect. Small variations in the channel dimensions in the PDMS molding should not effect our flow distribution and residence time predictions. Since each time point channel has the same dimensions, the major importance relies in the relative difference between the channels and tubing. This order of magnitude effect will not be influenced by micron-sized variations in the device fabrication process. To ensure this premise holds, the flow rates at each outlet were measured experimentally and validated.

Materials and methods

Device fabrication

This two-module device was fabricated using standard soft lithographic techniques.[29] Briefly, the modules were molded in poly(dimethylsiloxane) (PDMS) (Dow Corning Sylgard 184, Essex-Brownwell Inc., McDonough, GA) from a two-layer SU-8 (Microchem Corp., Newton, MA) master. One layer of 50 μm thick SU-8 2050 was spun onto 100 mm silicon wafer, baked, and exposed under UV light to define a negative image of the channel system in the resist. After baking to crosslink the exposed resist, another layer of 15 μm thick SU-8 2010 was spun on top. This layer formed the staggered herringbone array. After the same bake and expose process, the wafers were developed using propylene glycol monomethyl ether acetate (Doe & Ingalls, Inc., Durham, NC). The wafer was surface-treated with vapor-phase tridecafluoro-1,1,2,2-tetrahydrooctyl-1-trichlorosilane (United Chemical Technologies, Inc., Bristol, PA) for surface passivation. Then PDMS was cast on the SU-8 master and baked for 2 h at 70 °C. The PDMS was peeled off the mold and individual devices were cut to size. Medical grade polyethylene (PE) tubing (Scientific Commodities, Lake Havasu City, AZ) of various lengths and inner diameters were used for fluidic connections. Holes for fluidic connections were punched to a size determined by the outer diameter of the appropriate tubing.

Device operation

A syringe pump (Harvard Apparatus PHD 2000 Series Infusion) controlled the flow to the three inlets at 28.22 μL min^{-1} resulting in a 1/2 dilution of the stimulus and a 1/3 dilution of the lysis buffer. Because of this, the stimulus and lysis buffer were delivered at 2× and 3× concentration, respectively. The input cell concentration was $\sim 8 \times 10^6$ cells mL^{-1}. The resulting sample flow rates were 10.58 μL min^{-1}. For negative control, cell culture medium was first used in the place of the stimulation solution.

After the start of the flow, the fluid was flushed to waste for 9 min before sample collection. The time corresponded to that for the fluid front to get from the syringe to the end of the outlet tubing. The sample lysate effluent was collected for approximately 15 min to obtain 150 μL of sample, enough to perform all downstream analysis. To stimulate the cells, the process was repeated, with 2 μg mL^{-1} OKT3 antiCD3 diluted in media in place of cell culture medium inlet. The total amounts of reagents used for all eight time point sample collections included only 1.35 mL of cell suspension and lysis buffer, and 0.68 mL of media and stimulus. With improvements on the sensitivity of downstream analysis it is possible to collect far less lysate, thus conserving valuable sample.

Cells tend to settle over time because they are denser than the media that they are suspended in. The settling in the syringes and tubings causes cell loss during experiments and unreliable time data. Settling in the microfluidic channels causes the cells to roll along the bottom of the channel rather than follow the streamlines. To resolve this issue, the media and stimulation solutions were supplemented with dextran of ~70 000 MW (Sigma-Aldrich) to match the density of the cells (approx. 1.07 g cm^{-3}). The cell distribution after Module 1 was characterized by using only Module 1 with one inlet flowing medium containing cells at a know concentration and the other medium, both supplemented with dextran. The suspension in each outlet was collected and cells were counted to determine cell concentration.

Confocal microscopy

The confocal experiments were performed on a LSM 510 UV microscope (Carl Zeiss Inc.) with a 20× lens. Rhodamine-B dye at 0.05 mg mL^{-1} was used in one of the two entering streams. Inlets were perfused with the same flow rate as experimental conditions. The mismatch viscosity was created by using solutions of sucrose in water.[30]

Excitation was from a helium–neon laser (543 nm, 0.5 mW) and emission at 560 nm using a long pass wavelength filter optimized for Rhodamine-B. The pixel time was 1.6 μs with 2 μm slices in the z plane. Confocal images were used to evaluate the extent of mixing. After each cycle the standard deviation (σ) of intensity distributions of the channel cross-sections was used to quantify extent of mixing. A σ value of 0.5 signifies completely unmixed streams while a 0 value signifies completely mixed streams. For figure clarity the brightness and contrast were increased in the same way for all x–y projections.

Computational fluid dynamic models for the chaotic mixer

We modeled the transport and mixing in the HBM using the 3-D Navier–Stokes equations for flow and the diffusion–convection transport equation for the stimulant and the lysis buffer components at steady state. These equations were solved using COMSOL. Because of the asymmetry in the HBM, the model could not be reduced. However, the Navier–Stokes and convective diffusion equations can be decoupled and were solved separately. The vector form of the Navier–Stokes equations was as follows:

$$\rho\frac{\partial \boldsymbol{u}}{\partial t} - \mu\nabla^2\boldsymbol{u} + \rho(\boldsymbol{u}\cdot\nabla)\boldsymbol{u} + \nabla p = F \quad (5)$$

where ρ is the density, μ is the viscosity, $\boldsymbol{u}$ is the velocity vector, p is pressure, and F is a volume force field (gravity).

This solver assumes incompressible flow ($\nabla\cdot\boldsymbol{u} = 0$). The boundary conditions were assigned as parabolic flow profiles at a given average velocity for the inlets, zero pressure at the outlet, and non-slip on all remaining exterior boundaries. The interior boundaries were all assigned a neutral condition. These interior boundaries were created for enhanced 3-D mesh resolution by splitting the flow channel into eight subdomains and the herringbones into six subdomains each. This created additional mesh nodes inside the subdomain while allowing a continuous solution to the Navier–Stokes equations. The mesh density was such that further increases did not effect the convergence of the solution. The final mesh consisted of 65 000 elements with average quality >0.3.

Then using the velocity field from the solution of the Navier–Stokes equations, the non-conservative convective diffusion equations were solved

$$\delta_{ts}\frac{\partial c}{\partial t} + \nabla\cdot(-D\nabla c) = R - \boldsymbol{u}\cdot\nabla c \quad (6)$$

where δ_{ts} is the timescaling coefficient, equal to 1 when solving in the seconds timescale (this term will drop out at steady state), c is the concentration, D is the diffusion coefficient (~1×10^{-11} m^2 s^{-1} for protein molecules[31]), R is the reaction rate (set to zero in our model), and $\boldsymbol{u}$ is the 3-D velocity profile from the Navier–Stokes equations. The boundary conditions were assigned as $c = 1$ and $c = 0$ at each inlet, convective flux at the outlet, and insulation at all remaining exterior boundaries. The interior boundaries were all assigned a continuity condition.

Cell culture, cell lysis and protein analysis

For this study, we used Jurkat E6-1 human acute T cell lymphoma from ATCC (Manassas, VA, USA). Cells were cultured in RPMI 1640 medium with L-glutamine (Sigma-Aldrich) with 10 mM HEPES, 1 mM sodium pyruvate, and 1X MEM nonessential amino acids, and 100 units mL^{-1} penicillin streptomycin (Cellgro), supplemented with 10% certified heat inactivated fetal bovine serum (Sigma-Aldrich) at 37 °C in a humidified 5% CO_2 incubator. For the experiments, Jurkat cells were resuspended in a phenol-red free RPMI 1640 medium (Sigma-Aldrich), supplemented with the previous reagents and 0.3 mg mL^{-1} of L-glutamine (VWR) and 7 wt% dextran (Sigma-Aldrich). For the cell signaling experiments, the cells were treated with anti-human CD3, clone OKT3 (eBioscience) at a final concentration of 2 μg mL^{-1}. The lysis buffer used in these experiments was based on a 1% NP-40 solution (USBiological), supplemented with 1 M β-glycerophosphate (Calbiochem), 0.2 M sodium pyrophosphate (Alpha Aesar), 1 M sodium fluoride (EMD), 5 M Tris (Promega), 0.2 M sodium orthovanadate (Alfa Aesar), 5 M sodium chloride (Alfa Aesar), 100 mM benzamidine (Sigma), 500 mM EGTA (VWR), 5 mg mL^{-1} aprotinin (Sigma), 5 mg mL^{-1} leupeptin (VWR), 1 mg mL^{-1} pepsatin (Sigma), and 1 mg mL^{-1} microcystin-LR (Sigma).

For device-mediated cell lysing, lysis buffer at 0 °C was directly mixed with the cell suspension in Module 2 and lysate solution collected at the outlets of the device in microcentrifuge tubes. For standard bench lysing, the addition was made by pipette addition

of lysis buffer to microcentrifuge tubes containing the cells. For both forms of lysing, the samples were incubated on ice for 10–30 min, centrifuged at 14 000 rpm for 10 min and the supernatants were used for further analysis. The total protein concentration after lysis was determined with a BCA assay kit[32] and results were obtained after protein content between samples was diluted to uniform levels.

Stress and signaling

All analysis of phosphorylation dynamics were performed with a Bio-Plex-200 instrument (Bio-Rad) using commercially available Luminex bead assays. The phospho-JNK and phospho-p38 measurements (BioRad) or the quantification of proteins downstream of TCR (Beadlyte 7-plex Human T cell Receptor Signaling Kit, Millipore) were completed according to manufacturers' protocols. Results for all data are presented as the average of three independent sets of experiments. To adjust for baseline changes between experiment days, mean fluorescence intensity for each protein assay across samples was normalized by the maximum value for the data.

Results and discussion

Analysis of rapid mixing by microscopy and computational methods

The CFD modeling results and confocal images from experiments are shown in Fig. 2. In the confocal images [Fig. 2(c) and (d)], the bright fluorescent fluid is analogous to a stimulus rich solution and the dark areas are analogous to fluid with no stimulus. The experimentally determined profiles are similar to those by Stroock *et al.* under the same conditions.[24] More importantly, the computational model agrees well with experimental data [Fig. 2(e) and (f)]; hence the models can be used as a tool to probe the mixing properties and factors that may influence the extent of mixing to optimize our experimental conditions. Experimental results for mixing of solutions with the same viscosity (mimicking cell and stimulus mixing conditions) suggest that most cells would come into contact with the stimulus after 6 cycles because the widths of the stimulus-negative solution stream are smaller than the cell diameter ($\sim$ 10 μm); the standard deviation of pixel intensity is 0.14. After 9 cycles the solutions are completely mixed with a standard deviation of 0.05.

In contrast, when solutions with mismatched viscosity and density are mixed (as in the case of mixing cell suspension, $\mu \sim$ 4.3 cP and $\rho = 1.07$ g cm^{-3}, with lysis buffer, $\mu \sim 2.4$ cP and $\rho =$ 1.06 g cm^{-3}) with the same HBM, as seen in Fig. 3, the streamline profiles and hence the extent of mixing are qualitatively different. In this case, the mixing is slower and less efficient, marked by incomplete mixing after 9 cycles for mixing of solutions of 20 times viscosity mismatch. The standard deviation was 0.12. Although the viscosity and density of fluids are correlated in most cases, we can separate the two effects in the numerical simulations. Our models suggest that less effective mixing is mainly due to the mismatch in viscosity, not the difference in density, because the more viscous solution has a lower average velocity and therefore takes up more cross-sectional area [Fig. 3(c)]. This results in the fluid interface moving beyond the point of asymmetry (2/3 of the way across the channel) of the herringbones, reducing the effectiveness of the herringbones' ability to stretch, fold, and mix the two fluids. However, this effect occurs only at viscosity ratio of 6 : 1 and above for the current HBM design. Because we use dextran-supplemented solutions, we stay below the 6 : 1 viscosity ratio and therefore the HBM is adequate for fast mixing of cells and stimulus in Module 1, and of cells and lysis buffer in Module 2.

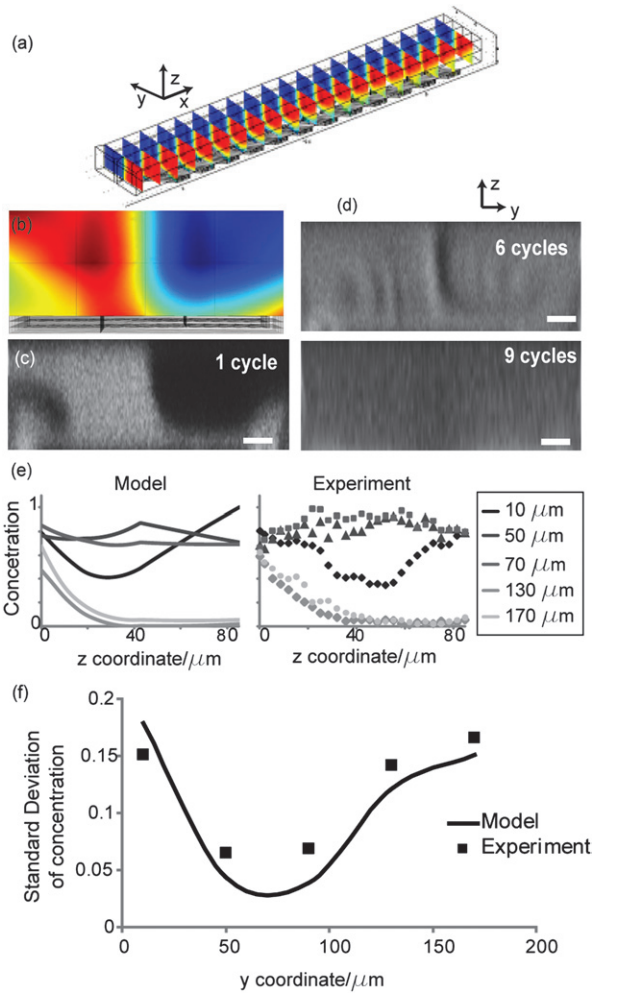

Fig. 2 Comparison of COMSOL model results with experiment. (a) Perspective view of the mixing for 1 cycle of herringbone mixers. The slices are in the y–z plane perpendicular to the direction of flow. (b) y–z plane of the concentration profile color map from the model after 1 cycle. Under the color map the z component of the herringbones are illustrated. (c) y–z view of a confocal image of mixing after 1 cycle with one inlet containing rhodamine dye. (d) y–z mixing profile after 6 and 9 cycles. The scale bar is 20 μm, twice the average diameter of a T cell. (e) Comparison of mixing profiles in the cross-section. Each line represents the normalized concentration profile in the z direction at the designated distances in the y direction from the wall. (f) Standard deviation of concentration across each line in (e).

The model was also used to characterize the shear stress at the walls. At the channel wall, the highest shear stress is $\sim$6 Pa and the highest shear stress at the herringbone wall is $\sim$1.8 Pa. These numbers are on the same order as those in the blood, with maximum shear stress of approximately 4 Pa.[33]

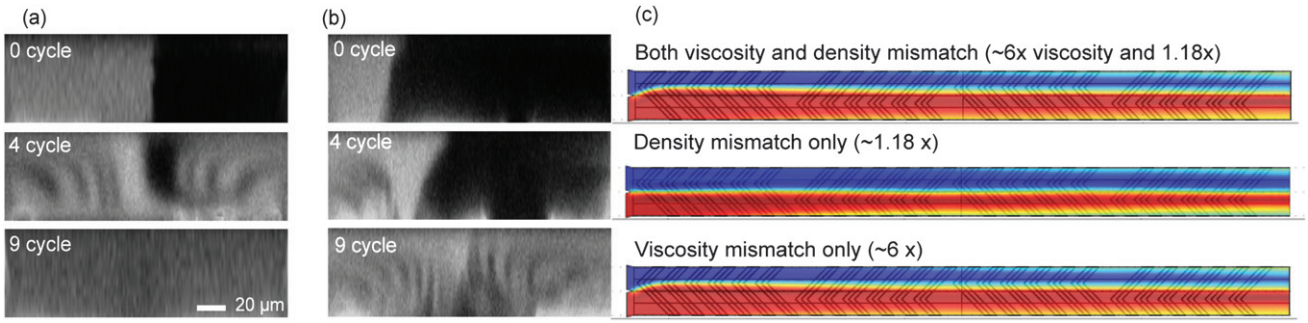

Fig. 3 Comparison of mixing of different viscosity solutions. (a,b) Confocal images of the cross-section at increasing mixing cycles of herringbones. One inlet contains fluorescent rhodamine dye. (a) *y*–*z* cross-sectional view of the mixing of two fluids with the same viscosity. (b) *y*–*z* cross-sectional view of the mixing of two fluids with mismatched viscosity; the fluid with no fluorescent dye has a viscosity 20 times the other. (c) Top view in the *x*–*y* plane of COMSOL data for density and viscosity mismatched solutions. The viscosity and density values are based on the sucrose solutions used with 6× the viscosity of water.

Tight control of stimulation times in multiple parallel samples

Based on the channel dimensions and fluid flow rates of the optimized setup, the staggered herringbone array achieved full mixing of reagents with minimal shear in less than 0.2 s on the stimulation chip (Module 1), and <0.9 s on the lysis chip (Module 2). These times are less than 5 percent of the ~23 s stimulation time, which was the shortest stimulation time in our experiments. Hence, the mixing time does not significantly affect our time point data.

Taylor dispersion, caused by diffusion and the parabolic flow profile, could be important for the cell stimulation time. With a diffusion coefficient on the order of 10^{-10} cm^2 s^{-1} (from Stokes–Einstein's equation), the modified Peclet number (ratio of the shortest residence time to the timescale for dispersion) is on the order of 10^5, suggesting that Taylor dispersion in the tubing will introduce errors in the stimulation/incubation time. However as we demonstrate in the protein signaling experiments in this work, the time points resolve easily and a trend can be quantified. If necessary, further experiments to determine the true residence time distribution can be used to deconvolve such time-series data, or an alternative incubation strategy can be used. For example, multiple chips with long channels of different volumes and also with integrated herringbone structures can be used in place of tubing, and may tighten the residence time distribution of the samples.

Flow resistance balance to achieve equal distribution of fluids

The flow rate in each outlet was characterized as described in the experimental methods section. Fig. 4(a) shows the flow rates across different time points with varying tubing dimensions. Error bars represent the standard deviation from trial to trial, which demonstrates the repeatability from device to device. The flat trend and tight standard deviation around the target 8.3 μL min^{-1} flow rate demonstrates the reliability of the device flow rates even while varying length, widths, and thus resistance (analogous to pressure drop) of the tubing (as shown it Table 1) between Modules 1 and 2 for each point. The highest pressure drops in the tubing is 66 Pa, as compared to 18 kPa in the microfluidic channels. The advantage is that this configuration provides large flexibility of the specific time points for stimulation we can achieve. With commercially available tubings, we can easily achieve stimulation times ranging from ~20 s to 1 h.

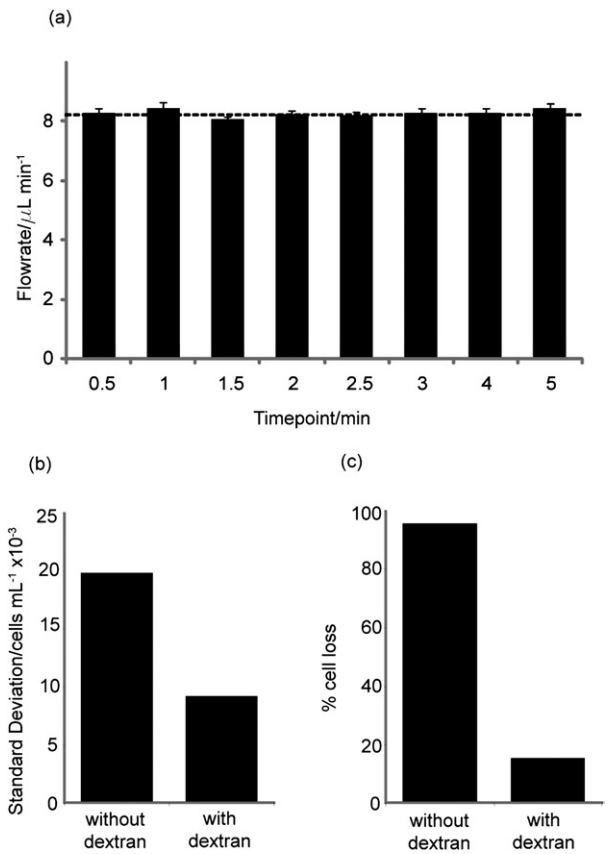

Fig. 4 Demonstration of device uniformity. (a) Equal flow rates in μL min^{-1} across the different channels. The channels are noted with the corresponding stimulation time in minutes. The dashed line indicates the set flow rate (total/number of channels) and error bars indicate standard deviation. (b) The average standard deviation of cell concentration in each stream with and without dextran supplement in the solutions. The standard deviation between experiments is decreased by half with the addition of dextran and percent cell loss is markedly decreased.

Table 1 Example tubing dimensions for given time points and the pressure drop for each tubing

Time point/min	Tubing ID/μm	Tubing length/cm	ΔP/Pa
0.5	280	4.2	66.4
1	380	4.7	21.9
1.5	580	3	2.6
2	580	4.1	3.5
2.5	580	5.2	2.6
3	580	6.2	3.1
4	580	8.3	4.2
5	580	10.4	5.3

Reliable cell distribution after stimulation and reliable protein yield after lysis

Without adding dextran to the cell suspension, cells were often observed to settle and aggregate; these aggregations in turn cause blockage on chips and together with settling cause the cell distribution in the eight collected samples to be non-uniform and unpredictable. In comparison, reliable cell distribution between experiments was achieved by adding dextran to the solutions for density matching. In addition, dextran may also contribute to the suppression of non-specific adsorption of serum proteins in the medium, which promotes cell adhesion to the device walls. As shown in Fig. 4(b), the average standard deviation of cell density in each stream was decreased by more than half. These data were obtained by flowing cells through the device at a known density, but replacing the stimulus and lysis solutions with media, and counting intact cells from each outlet. In addition, by taking the cells lost [Fig. 4(c)] to settling in the syringes and devices into account, the resulting improvement by adding dextran is very significant. Although variability between cell concentrations per stream still exists, protein activity data can be easily normalized by the total protein in the sample. We have verified that the total protein yield is linearly correlated to the number of cells in the sample (data not shown).

On-chip cell handling showing minimal stress on cells

For a microfluidic device to perform optimally for signal-transduction applications, fluid forces must not impose adverse stresses on the cells within the chip. To validate that the cells flowing through the device were not subjected to undesirable shear stress due to fluid flow in narrow channels, undesirable mechanical forces produced by chaotic mixing, or lack of oxygen perfusion during the course of the experiment, the phosphorylation state of two MAPK proteins associated with stress response, p38 and JNK, were monitored. Cells in dextran-supplemented medium (no stimulatory reagents) were pumped through Module 1 and lysed in Module 2. The lysates were compared to the results from cells lysed by an analogous bench-top protocol (also without any stimulation). As shown in Fig. 5, the levels of p38 and pJNK activation for the on-chip experiment are constant over time and comparable to the results obtained on bench, demonstrating that the cells are neither adversely stressed by the conditions imposed by flow through the microchannels, nor stressed by the time spent in the tubings. There was no noticeable change in cell viability or morphology as observed by trypan blue exclusion after cells were subjected to flow through the device (data not shown).

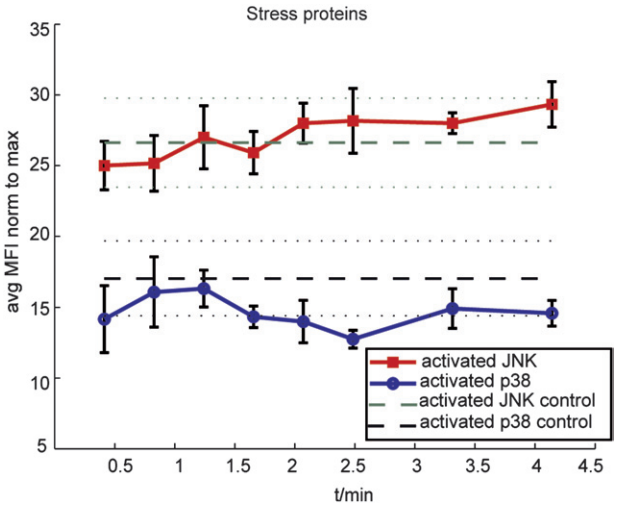

Fig. 5 Activated JNK and p38 concentrations in cells collected from the microfluidic devices compared to on bench controls, showing no signs of cellular stress induced by the device. For this experiment, samples were normalized to total cellular protein content. The experiments were run with three different devices and then the protein phosphorylation quantification was obtained with duplicates. Dashed lines represent the quantified values for phospho-p38 and phospho-JNK from control samples lysed on the bench. Dotted lines indicate standard deviation associated with the control values. Mean fluorescence intensity measurements for positive controls were comparable in magnitude to positive control lysates supplied by the manufacturer (data not shown).

Parallel on-chip experiments for high-throughput multi-time point protein activation assays

The temporal regulation of protein activation during T cell receptor signaling involves multiple coordinated feedback loops, as reviewed by Germain *et al.*[10] Prior proteomic studies indicate that widespread phosphorylation of signaling molecules occur within 5 min of T cell activation;[34] thus, a method for consistent generation of sub-minute signaling events would be useful for extracting relationships between interconnected network components. To ensure that the microfluidic system is a reliable method of evaluating T cell activation, we characterized the phosphorylation dynamics of representative signaling molecules downstream of the T cell receptor [Fig. 6(a)]. Comparisons between anti-CD3 (OKT3) stimulated Jurkat lysates generated by standard bench-top protocol and those generated by the device were made using the Beadlyte 7-plex human T cell receptor phosphoprotein signaling kit (Upstate). This kit quantifies phosphorylated ITAMs (CD3ε), Zap-70, Lck, LAT, Erk, and CREB using the Luminex instrument as described by Khan *et al.*[35] Jurkat cells in a 7% dextran medium were stimulated with the soluble form of anti-CD3 for the incubation times ranging approximately from 20 s to 4.5 min and then lysed with a cold lysis buffer containing phosphatase and protease inhibitors that prevent further biochemical events after lysis. Fig. 6(b)–(g) show the signaling dynamics for these six proteins of interest for lysates generated by the microfluidic device and for lysates generated on

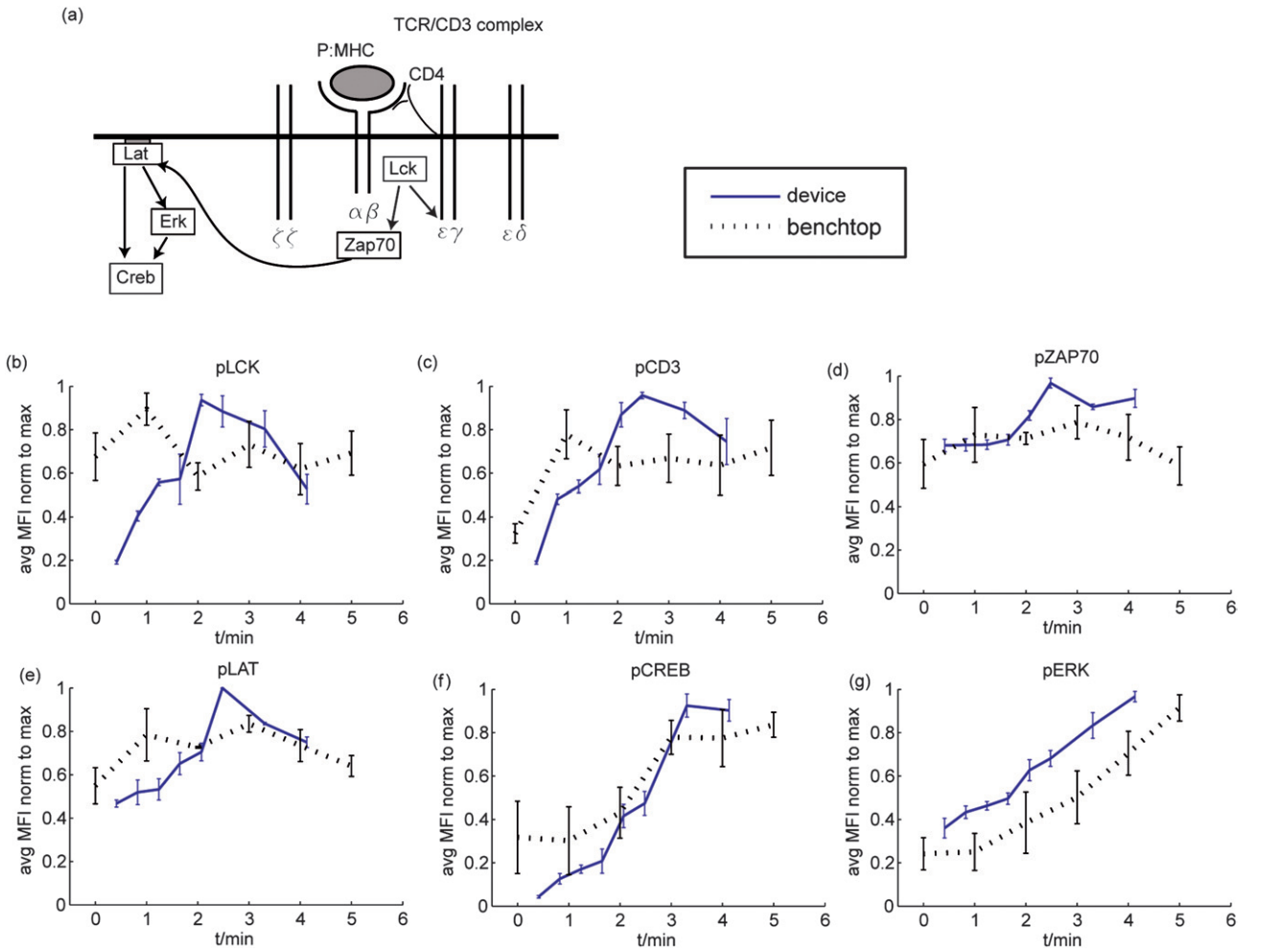

Fig. 6 (a) Simplified pathway of TCR activation. After a peptide MHC has bound to the CD3/TCR complex, Lck phosphorylates the ITAM CD3, which recruits the tyrosine kinase Zap-70 to the complex. Zap-70 phosphorylates then the adaptor protein LAT that activates the MAPK and the Ras pathway, the latter enabling the activation of Erk and CREB. In our case, we used OKT3 that specifically reacts with the CD3 complex. (b–f) For each of the selected protein, comparison of the dynamics obtained with the microfluidic device and those obtained by standard bench-top protocol. The dynamics are very similar and the microfluidic device shows a better consistency in the results.

bench. As illustrated in the simplified scheme of the TCR signaling cascade [Fig. 6(a)], the first proteins to be phosphorylated are CD3, Lck and Zap-70. Multiple signaling events occur before the downstream adaptor LAT, and the kinases Erk and CREB, are phosphorylated.

With the device, phosphorylation of CD3, Lck and Zap-70 starts after 2 min of stimulation and reaches its peak at 3 min. In contrast, the phosphorylation of Erk rises concurrently with the downstream protein CREB over a longer period of 5 min. As expected, smaller variation occurs among samples across repeated experiments with the microfluidic device than with the manual stimulation and lysing, demonstrating a tight control over cell handling on-chip. The dynamic trends of activation are not dissimilar between the two experimental methods; however, an important feature emerges from the data. The uniformity of stimulatory exposure results in higher magnitudes of phosphorylation at early time points for all proteins measured. This is especially evident in the CD3 ITAM phosphorylation, possibly due to a flattened distribution of stimulated cells in the manual bench-top samples arising from the time lag of antibody : cell mixing. This feature highlights the necessity of consistent sample handling when quantifying cell population averages for signaling dynamics, especially when using small numbers of cells.

Conclusions

Our device successfully accomplishes a multi-time point stimulation experiment with on-chip cell lysis. Rapid mixing, achieved with the staggered herringbone array, allows precise time point resolution down to 20 s. Modeling and confocal mixing experiments gave valuable insight into the mixing of solutions, with a wide range of fluidic properties, relevant to biological experiments. The flexible nature of this modular design allows easy adjustment of time points without changing the device or operation conditions. This one-time-use device is inexpensive to fabricate, simple to set up, and simple to use. The flexibility and potential for automation in the microfluidic format allows for future development for more "online" processing of samples, which may further reduce necessary sample volumes and cell concentrations. From a single experiment, six proteins were

analyzed simultaneously for eight time points, yielding 48 measurements from only 10 million cells, only 5% of the amount needed in conventional methods.[7] We expect a high-throughput format of this device coupled with multiplexed biochemical analysis to yield large sets of quantitative data for reconstructing signaling networks in many applications.

References

1 K. A. Janes, J. G. Albeck, S. Gaudet, P. K. Sorger, D. A. Lauffenburger and M. B. Yaffe, *Science*, 2005, **310**, 1646–1653.
2 T. Reya and H. Clevers, *Nature*, 2005, **434**, 843–850.
3 C. Sander, *Science*, 2000, **287**, 1977–1978.
4 J. B. Gibbs, *Science*, 2000, **287**, 1969–1973.
5 S. Gaudet, K. A. Janes, J. G. Albeck, E. A. Pace, D. A. Lauffenburger and P. K. Sorger, *Mol. Cell. Proteomics*, 2005, **4**, 1569–1590.
6 B. Schoeberl, C. Eichler-Jonsson, E. D. Gilles and G. Muller, *Nat. Biotechnol.*, 2002, **20**, 370–375.
7 M. L. Kemp, L. Wille, C. L. Lewis, L. B. Nicholson and D. A. Lauffenburger, *J. Immunol.*, 2007, **178**, 4984–4992.
8 H. E. Kohrt, C. T. Shu, T. B. Stuge, S. P. Holmes, J. Weber and P. P. Lee, *J Immunother*, 2005, **28**, 297–305.
9 B. N. Kholodenko, O. V. Demin, G. Moehren and J. B. Hoek, *J. Biol. Chem.*, 1999, **274**, 30169–30181.
10 R. N. Germain and I. Stefanova, *Annu. Rev. Immunol.*, 1999, **17**, 467–522.
11 K. Sachs, O. Perez, D. Pe'er, D. A. Lauffenburger and G. P. Nolan, *Science*, 2005, **308**, 523–529.
12 J. El-Ali, P. K. Sorger and K. F. Jensen, *Nature*, 2006, **442**, 403–411.
13 A. Groisman, C. Lobo, H. J. Cho, J. K. Campbell, Y. S. Dufour, A. M. Stevens and A. Levchenko, *Nat. Methods*, 2005, **2**, 685–689.
14 S. Paliwal, P. A. Iglesias, K. Campbell, Z. Hilioti, A. Groisman and A. Levchenko, *Nature*, 2007, **446**, 46–51.
15 K. R. King, S. Wang, A. Jayaraman, M. L. Yarmush and M. Toner, *Lab Chip*, 2008, **8**, 107–116.
16 J. El-Ali, S. Gaudet, A. Gunther, P. K. Sorger and K. F. Jensen, *Anal. Chem.*, 2005, **77**, 3629–3636.
17 H. Lu, M. A. Schmidt and K. F. Jensen, *Lab Chip*, 2005, **5**, 23–29.
18 M. A. McClain, C. T. Culbertson, S. C. Jacobson, N. L. Allbritton, C. E. Sims and J. M. Ramsey, *Anal. Chem.*, 2003, **75**, 5646–5655.
19 C. E. Sims and N. L. Allbritton, *Lab Chip*, 2007, **7**, 423–440.
20 P. J. Lee, P. J. Hung, V. M. Rao and L. P. Lee, *Biotechnol. Bioeng.*, 2006, **94**, 5–14.
21 D. D. Carlo, C. Ionescu-Zanetti, Y. Zhang, P. Hung and L. P. Lee, *Lab Chip*, 2005, **5**, 171–178.
22 A. E. Herr, A. V. Hatch, D. J. Throckmorton, H. M. Tran, J. S. Brennan, W. V. Giannobile and A. K. Singh, *Proc. Natl. Acad. Sci. U. S. A.*, 2007, **104**, 5268.
23 A. P. Sudarsan and V. M. Ugaz, *Proc. Natl. Acad. Sci. U. S. A.*, 2006, **103**, 7228–7233.
24 A. D. Stroock, S. K. W. Dertinger, A. Ajdari, I. Mezic, H. A. Stone and G. M. Whitesides, *Science*, 2002, **295**, 647–651.
25 P. B. Howell, D. R. Mott, S. Fertig, C. R. Kaplan, J. P. Golden, E. S. Oran and F. S. Ligler, *Lab Chip*, 2005, **5**, 524–530.
26 J. T. Yang, K. J. Huang and Y. C. Lin, *Lab Chip*, 2005, **5**, 1140–1147.
27 D. R. Mott, P. B. Howell, J. P. Golden, C. R. Kaplan, F. S. Ligler and E. S. Oran, *Lab Chip*, 2006, **6**, 540–549.
28 *Fluid Mechanics*, F. M. White, McGraw-Hill Publishers, New York, 4th edn, 1999, p. 365.
29 Y. N. Xia and G. M. Whitesides, *Annu. Rev. Mater. Sci.*, 1998, **28**, 153–184.
30 M. Migliori, D. Gabriele, R. Di Sanzo, B. de Cindio and S. Correra, *J. Chem. Eng. Data*, 2007, **52**, 1347–1353.
31 W. M. Deen, *Analysis of Transport Phenomena*, Oxford University Press, Inc., New York, 1998.
32 L. T. Lam, R. E. Davis, J. Pierce, M. Hepperle, Y. Xu, M. Hottelet, Y. Nong, D. Wen, J. Adams, L. Dang and L. M. Staudt, *Clin. Cancer Res.*, 2005, **11**, 28–40.
33 S. P. Wu, S. Ringgaard, S. Oyre, M. S. Hansen, S. Rasmus and E. M. Pedersen, *J. Magnetic Resonance Imaging*, 2004, **19**, 188–193.
34 J. E. Kim and F. M. White, *J. Immunol.*, 2006, **176**, 2833–2843.
35 I. H. Khan, S. Mendoza, P. Rhyne, M. Ziman, J. Tuscano, D. Eisinger, H. J. Kung and P. A. Luciw, *Mol. Cell. Proteomics*, 2006, **5**, 758–768.